International Journal of Computational Methods and Experimental Measurements
https://www.acadlore.com/journals/IJCMEM

Modeling Bed Morphology Evolution in an Alluvial River under Extreme Rainfall Using a 2D Hydrodynamic–Sediment Transport Approach

I Gede Tunas[1*], Puji Harsanto[2], Yassir Arafat[1]

[1] Department of Civil Engineering, Faculty of Engineering, Universitas Tadulako, 94117 Palu, Indonesia
[2] Department of Civil Engineering, Faculty of Engineering, Universitas Muhammadiyah, 55183 Yogyakarta, Indonesia

[*] Correspondence: I Gede Tunas (tunasw@yahoo.com)

Received: 08-07-2025 **Revised:** 09-10-2025 **Accepted:** 09-25-2025

Citation: I. G. Tunas, P. Harsanto, and Y. Arafat, "Modeling bed morphology evolution in an alluvial river under extreme rainfall using a 2D hydrodynamic–sediment transport approach," *Int. J. Comput. Methods Exp. Meas.*, vol. 13, no. 3, pp. 667–679, 2025. https://doi.org/10.56578/ijcmem130315.

Abstract: Extreme precipitation events driven by climate change significantly accelerate sediment delivery into alluvial rivers, resulting in substantial morphological alteration and downstream channel instability. This study investigates bed evolution within the downstream segment of the Palu River in Central Sulawesi, Indonesia, by applying a two-dimensional hydrodynamic and sediment transport model in HEC-RAS 2D. Three discharge scenarios representing dry, wet, and extreme rainfall conditions were simulated using river geometry derived from high-resolution DEM and bathymetric measurements. Model performance was calibrated against observed water levels, achieving optimal agreement at a Manning's roughness coefficient of 0.0295 with a Root Mean Square Error of 0.15. The results demonstrate pronounced spatial variability in riverbed response. Under extreme rainfall, degradation is dominant in the upstream bend zone with maximum erosion depth reaching 0.40 m, while deposition intensifies near the river mouth, producing aggradation up to 0.75 m. Although the spatial patterns remained consistent across all simulated scenarios, the magnitude of morphological change during extreme rainfall reached approximately twice that observed under wet-season discharge. These findings highlight the critical role of extreme flow events in shaping alluvial river morphology and provide essential quantitative benchmarks for river management strategies targeting flood mitigation and navigation safety.

Keywords: Alluvial river morphology; Extreme rainfall; Sediment transport modeling; HEC-RAS 2D; Bed aggradation and degradation; Hydrodynamic simulation

1 Introduction

Degradation and aggradation are two forms of alluvial riverbed morphology resulting from the interaction between flow, sediment, and river geometry [1]. Sediment transported by flow can be deposited along a river section if deposition conditions are met, which are determined by flow velocity, which depends on the river's discharge and geometry [2]. The riverbed becomes higher than its previous elevation due to the deposition of this sedimentary material, causing the slope of the riverbed to change. Conversely, if the kinetic energy of the flow is greater than the resistance of the riverbed, the riverbed will erode [3]. The kinetic energy of the flow is highly dependent on flow velocity, with alluvial riverbeds being relatively easily eroded by this energy due to the characteristics of the grains forming them, which are alluvial sediments, which are generally loose materials with low cohesiveness [4]. The strength of the bonds between sediment grains represents the riverbed's resistance to resisting the kinetic energy of the flow. Riverbed erosion over a long period can cause riverbed degradation, the opposite of aggradation [5]. Under certain conditions, transport equilibrium can be achieved when the rate of sediment inflow equals the rate of sediment outflow at the river point being studied.

The bed morphology of alluvial rivers is generally dynamic and can change over time depending on various factors: the amount of transported sediment supplied by erosion throughout the catchment, including the river channel; the flow velocity that creates kinetic energy for the erosive nature of the river bed; the hydraulics of structures built perpendicular to or parallel to the streamline, such as weirs, dams, check dams, ground sills, groynes, and others; and the influencing flow conditions at the downstream end, such as tides [6]. However, the first two main factors are the most dominant factors determining changes in bed morphology. The characteristics of transport rates that influence bed morphology along alluvial river sections vary and differ. In the upstream segment, the high-gradient section is generally a scour zone where the riverbed is dominated by large rock material with a narrow cross-section and deep channels. Furthermore, in the middle segment, the riverbed slope decreases, with bed material dominated by medium-sized rocks and gravel. Flow velocity in this segment weakens in line with the decreasing slope of the riverbed. This middle segment is generally a transport equilibrium segment where the riverbed morphology is relatively stable. Finally, the downstream segment is a deposition zone with a very low riverbed slope. This sedimentation zone is characterized by high sediment deposition due to very low flow velocities.

Due to the complex issues caused by aggradation and degradation, particularly changes in river cross-sectional capacity that trigger flooding, changes in riverbed morphology must be controlled. Several methods can be applied to control it, but at least three are particularly important [7]. The first is to control the rate of erosion on the ground surface throughout the catchment by maintaining forest cover, converting open land back to forest, and managing dryland farming systems by implementing terracing systems following land contour lines [8]. The second method is to control scour along riverbanks by strengthening riverbanks with revetments and directing flow using groynes. Scour locations on riverbanks are generally found on the outer side of bends where flow velocities are higher than on the inner side of the bend. The final main method is to control the rate of sediment transport and bed stability by constructing sabo dams, check dams, and ground sills.

Several researchers have conducted studies and published papers in journals related to bed morphology modeling and control strategies, particularly those triggered by extreme rainfall. The first group of researchers examined sediment produced by climate change and extreme rainfall that trigger debris flows in rivers [9, 10]. Climate change can trigger increased sediment production and debris flows in rivers due to increased erosion rates on the catchment surface. The next group of researchers studied the interaction between flow and river geometry, as conducted by Van Appledorn et al. [11] and Reisenbüchler et al. [12]. Flow fluctuations play a significant role in influencing river morphological changes with a high correlation. Furthermore, Himayoun and Roshni [13], Stähly et al. [14], and Liu et al. [7] also studied geomorphic changes and sediment deposition due to floods triggered by extreme rainfall. Sediment deposition that causes geomorphic changes is influenced by river flow fluctuations. The last group focuses on the study of erosion, deposition, and morphological changes under the influence of extreme floods and tides [15–17].

This series of studies demonstrates that studies on sediment transport and riverbed morphology are highly advanced. However, these studies have not yet demonstrated a comparison of bed morphology changes with normal discharge conditions. Moreover, trends in bed morphology change, particularly in alluvial rivers, under various trigger scenarios have not been studied in published studies. Therefore, trigger factors scenario represents a novelty in this study, emphasizing the rate of bed morphology change under dry season, rainy season, and extreme rainfall conditions.This study aims to examine bed morphology changes in alluvial rivers due to extreme rainfall using 2D visualization.

2 Material and Methods

2.1 Study Area

The approximately 5 km downstream segment of the Palu River, the site of this research, is located in Palu City, Central Sulawesi Province, Indonesia (Figure 1). This river is one of the largest alluvial rivers in the province, with a catchment area of over 3,000 km^2, and a main river length of no less than 100 km [18, 19]. Sediment deposited at the river mouth originates from two main tributaries, the Miu and Gumbasa, and is further supplied by dozens of supporting tributaries, including several debris rivers such as the Sombe-Lewara, Poi, and Bangga [20].

Sediment deposition, primarily in the downstream section, causes shallowing of the river bed due to low flow velocities far below the critical bed frictional stress of sediment grains [21]. Tides also play a significant role in influencing sediment deposition, particularly during high water levels, which create flow stagnation that causes backwater to flow upstream [22]. This process occurs alternately following flow fluctuations, so that bed morphological changes occur very dynamically over time [23, 24].

Sediment deposits in downstream rivers generally originate from ground surface erosion throughout the catchment [25]. Runoff and erosion rates are specifically influenced by various physical factors in the catchment, including topography, land cover and use (LULC), and soil texture [26–28]. The Palu watershed has a topography with elevations ranging from 0 to 2,500 m above sea level, with a relatively even distribution of elevations throughout the catchment (Figure 2a). This topographic distribution forms varying slope gradients, dominated by moderate slopes below 30%. Over time, some land cover has been converted from forest to plantations, agriculture, residential areas, and urban areas. The red color of the land cover, as shown in Figure 2b and Figure 2c, indicates the massive growth of settlements due to urban development, especially in Palu City. The impact of this land conversion is predicted to affect runoff rates, which trigger erosion on the ground surface. In addition, the Palu watershed is dominated by alluvial soil types throughout almost the entire Palu Valley, consisting of sand, clay, and silt textures (Figure 2d). Several other types are seen in other parts of the catchment, especially along the left and right edges of the catchment, such as Latosol, Mediterranean, Regosol, and Podzolic.

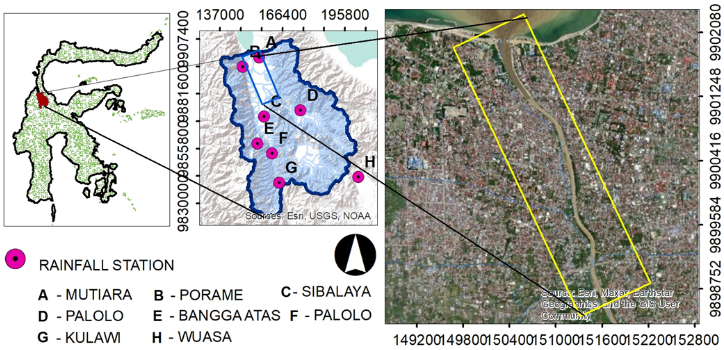

Figure 1. Detail location of study area

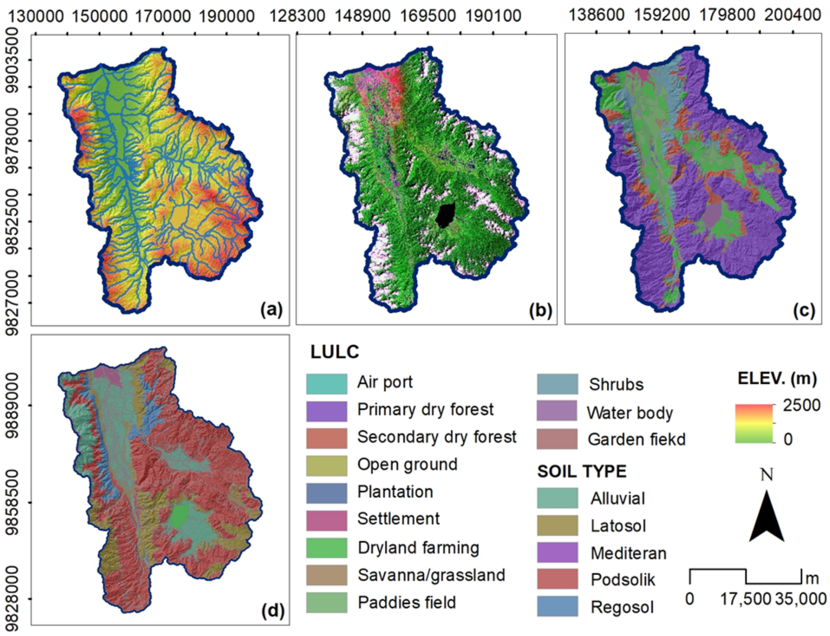

Figure 2. Characteristics of Palu catchment: (a) DEM; (b) Landsat image; (c) LULC; (d) Soil type

The development of changes in the bed morphology of this alluvial river can be observed directly at the research site or through satellite imagery [29]. Based on Google Earth imagery, one of the points of massive sedimentation is located upstream on the right side of the Palu II Bridge (Figure 3). Observations from three years of data: 2019, 2022, and 2024, show that sedimentation begins with light deposition when the discharge is low (Figure 3a). As the discharge fluctuates with a number of sediment concentrations, deposition occurs more intensively and more compactly, as shown in Figure 3b. This sediment deposition then forms a plain along the riverbank, which can affect the river's cross-sectional capacity (Figure 3c).

Furthermore, more detailed changes in the riverbed morphology can be observed in the river mouth segment (Figure 4). In the period 2019–2024, it is indicated that sedimentation has occurred massively at the river mouth. Dominant fine sediments are seen spreading beyond the river mouth (Figure 3a), which also settle around Palu Bay under the influence of tides, currents, and waves. These deposits then develop and form a delta-like bar, as shown in Figure 2b and Figure 3c. Silting in this area often causes riverbank overflows, especially during major floods. Routine maintenance is essential to maintain the river's cross-sectional capacity.

Figure 3. Morphology of river bends at the upstream of Palu II Bridge: (a) May 2019; (b) September 2022; (c) April 2024

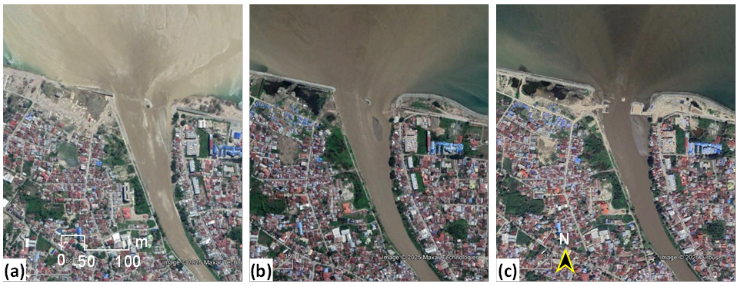

Figure 4. Morphology of river mouth: (a) May 2019; (b) September 2022; (c) April 2024

2.2 Data

Investigation and data collection are essential to support this research. Data can be grouped into two components: secondary data and primary data. These data comprises basic data for HEC-RAS2D modeling, including DEM data of the study area to construct river geometry (Figure 5a), extreme rainfall data and its transformed hydrographs (Figure 5b and Figure 5c), and tidal data (Figure 6a). DEM data was obtained from terrestrial and bathymetric measurements approximately 5 km upstream, as a result of a combined survey using Geodetic GPS and an echosounder with a final resolution of less than 2 meters. Limited data on land was further enhanced with aerial drone data, particularly for areas not covered by terrestrial measurements. All of these data are combined using Kriging interpolation techniques to standardize the DEM resolution. Input data for modeling flow and changes in river bed morphology are presented in Figure 5.

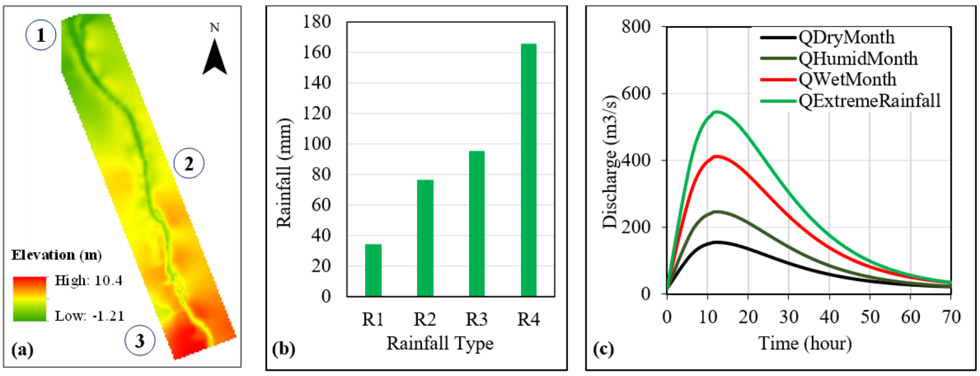

Figure 5. Flow and sediment modeling data: (a) DEM; (b) Rainfall; (c) Hydrograph

Daily rainfall data for a 10-year period as the basis for determining the hydrograph is divided into four types, namely average rainfall in dry months, average rainfall in humid months, average rainfall in wet months and extreme rainfall (Figure 5b) with peak hydrograph discharges in sequence: 153.45 m^3/sec, 245.14 m3/sec, 410.42 m^3/sec, and 545.24 m^3/sec. Rainfall discharge transformation is performed using the HEC – HMS Model. Meanwhile, tidal data is the result of hourly water level measurements in the period from August 28, 2025 to September 11, 2025 for 15 days (Figure 5c). The results of tidal harmonic analysis using the time series data produce a maximum water level of 2,002 m.

Another important data used for modeling bed morphology changes is bed sediment data. This data was obtained through direct measurements at the midpoint river of the Palu 2 Bridge using a bed load grab sampler (Figure 6a). These samples were then examined for grain size distribution at the Structural Laboratory of Tadulako University using the sieve analysis method, with the results presented in Figure 6b. The measured sediment grain gradation is generally dominated by fine sand and a small portion of medium sand. This grain size decreases downstream, where it moves as suspended load and settles as a sediment bed.

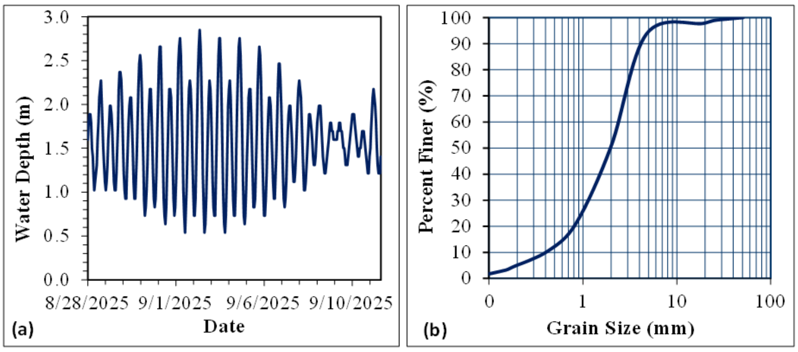

Figure 6. Tidal fluctuation at the (a) Palu River estuary; (b) sediment grain gradation size

2.3 Sediment Transport

Changes in bed morphology depend on the total sediment transport in the river, which consists of two components: bed sediment transport and suspended sediment transport. The first component represents bed sediment transport which is expressed by [30]:

$$\frac{\partial}{\partial t}\left(\frac{hC_{bk}}{\beta_{bk}}\right) = \nabla \cdot (\varepsilon_{bhk} h \nabla C_{bk}) + E_{bk} - D_{bk} - \nabla \cdot \{h\,(U + U_{bn})\,C_{bk}\} \tag{1}$$

where, $\frac{\partial}{\partial t}$ is partial derivative operator, h is water depth (m), C_{bk} is concentration of bed-load sediment (kg/m^3), β_{bk} is correction factors of bed-load, ∇ is vector differential operator, ε_{bhk} is horizontal diffusion coefficient of bed-load (m^2/s), E_{bk} is erosion rate of bed-load (kg/m^{2}s), D_{bk} is deposition rate of bed-load (kg/m^{2}s), U is current velocity of depth-averaged (m/s), and U_{bn} is correction velocity of bedload secondary flow (m/s).

The second component of total transport is suspended sediment transport (q_{sk}) which is formulated with:

$$q_{sk} = hUC_{sk} \tag{2}$$

where, C_{sk} is local fraction suspended sediment concentration (kg/m^3). The combination of bed load and suspended load becomes the total load which is expressed as:

$$\frac{\partial}{\partial t}\left(\frac{hC_{tk}}{\beta_{tk}}\right) = \nabla \cdot (\varepsilon_{tk} h \nabla C_{tk}) + E_{tk}^{HF} - D_{tk}^{HF} + S_{tk} - \nabla \cdot (hUC_{tk}) \tag{3}$$

where, C_{tk} is concentration of total-load sediment (kg/m^3), β_{tk} is correction factors of total-load, ε_{tk} is horizontal diffusion coefficient of total-load (m^2/s), E_{tk}^{HF} is erosion rate of total-load in hydraulic flow (kgm^2/sec), D_{tk}^{HF} is deposition rate of total-load in hydraulic flow (kg^2/sec), and S_{tk} is source $/$sink total-load term (kg^2/sec).

2.4 Bed Morphology Change

The concept of bed morphology change is based on the assumption that the river bed consists of a number of layers, where elevation changes start from the topmost layer. Total and fractional riverbed morphological changes in HEC-RAS 2D are formulated with the following equation:

$$\frac{\partial_{zb}}{\partial t} = \sum_k \left(\frac{\partial_{zb}}{\partial t}\right)_k \tag{4}$$

$$\left(\frac{\partial_{zb}}{\partial t}\right)_k = \frac{D_{tk} - E_{tk} + \nabla \cdot (\kappa_{bk} \left|q_{bk}\right| \nabla_{zb})}{\rho_{sk}(1-\phi_b)} \tag{5}$$

where, zb is bed elevation with relation to the vertical reference (m), t is time in second, k is size class (mm), $|q_{bk}|$ is magnitude of bed-load mass transfer (kg/m·s), ρ_{sk} is grain class particle density (kg/m^3) and ϕ_b is porosity of deposited and degraded materials. D_{tk} is deposition rate total load (kg/m^2·sec), E_{tk} is erosion rate of total load (kg/m^2·sec), and κ_{bk} is bed-slope coefficient of empirical grain class, &which are calculated by the equation:

$$D_{tk} = r_A^{HF} D_{tk}^{HF} \tag{6}$$

$$E_{tk} = f_{1k} E_{tk}^{*} \tag{7}$$

$$\kappa_{bk} = \kappa_{b0} \sqrt{\frac{\tau_{crk0}}{\max \tau_b', \tau_{crk0}}} \tag{8}$$

where, r_A^{HF} is horizontal area fraction corresponding to hydraulic flow, D_{tk}^{HF} is deposition rate of hydraulic flow (kg/m^{2}s), f_{1k} is class fractions of active grain by weight, E_{tk}^{*} is potential erosion rate (kg/m^{2}s), κ_{b0} is empirical parameter (0.1-0.5), τ_{crk} is critical shear stress (kg/m·sec^2) and τ_b' is bed skin shear stress (kg/m·sec^2). The rate of potential erosion consists of two basic formulas, namely hydraulic flow erosion and sheet and splash erosion, as follows:

$$E_{tk}^{*} = \underbrace{r_A^{HF} E_{tk}^{*HF}}_{\text{hydraulic flow erosion}} + \underbrace{r_A^{SS} E_{tk}^{*SS}}_{\text{sheet and splash erosion}} \tag{9}$$

HF dan SS respectively refer to hydraulic flow erosion and sheet and splash erosion.

2.5 Model Setup

Important components in morphological modeling are geometry, boundary conditions, and simulation time step. The model geometry is expressed as a 15 m × 15 m grid or mesh formed from DEM data. The grid size is based on the DEM resolution and affects numerical stability, simulation accuracy, and run time [31]. Numerical stability is achieved at a 1-minute time step and tends to be unstable at larger time intervals.

The boundary conditions assigned to the model are based on Figure 5c, Figure 6a, and Figure 6b. The flow hydrograph was assigned at the upstream boundary with three discharge categories: discharge during dry months, discharge during wet months, and discharge due to extreme rainfall (Figure 5c). Furthermore, sediment gradation data was also assigned at the upstream boundary of the model as a parameter determining bed morphology (Figure 6b). Finally, tidal fluctuations were assigned as the downstream boundary (Figure 6a) with a duration of 15 days.

3 Result and Discussion

3.1 Hydrodynamic Modeling

It has been previously confirmed that hydrodynamic simulations for river bed morphology change analysis are preceded by the calibration of the Manning roughness coefficient (n) which affects the velocity and depth of flow in the river. This stage is carried out based on the input discharge and the water level (Figure 7a) by assessing the difference between the observed water level and the simulated water level at the reference point (Figure 7b) using the Root Mean Square Error (RMSE). The calibration process is performed by repeatedly trialing the Manning roughness coefficient until obtaining the smallest RMSE approaching 0. This calibration scenario is presented in Figure 7 where the optimal n is 0.0295 with an RMSE of 0.15.

Various factors can influence the n parameter, primarily concerning the physical material conditions of the river cross-section, both the bed and the banks. However, in the context of flow hydrodynamics, this roughness parameter can change depending on the flow velocity. Friction between the riverbed/bank and the flow will increase as the flow velocity rises, and vice versa [16]. Therefore, the Manning roughness coefficient cannot be determined statically, considering that the interaction of the flow with the river cross-section always changes according to discharge fluctuations. In the case of the research location, the river bed material is dominated by fine-grained deposits such as silt and fine sand, especially at the riverbanks [21]. The type and size of the material tend to become coarser towards the center of the river cross-section. The bed material begins to mix with fine gravel and coarse gravel. This bed material characterizes and represents the type of bed material in the downstream segment of alluvial rivers such as the Palu River [23].

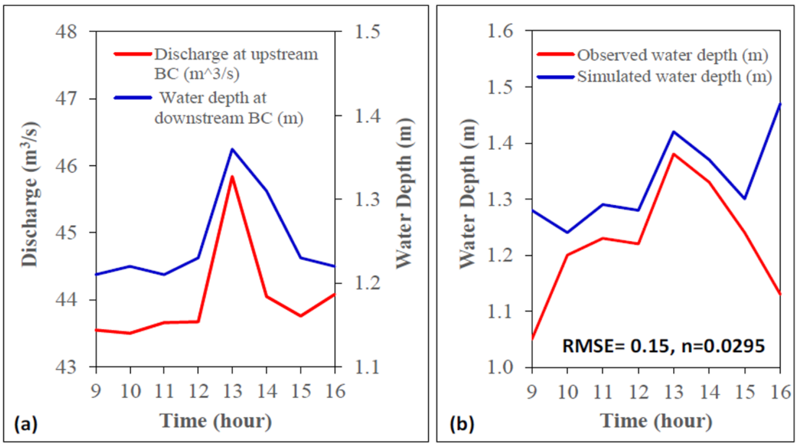

Figure 7. Boundary conditions for model calibration: (a) upstream and downstream boundary input; (b) controlled water level

3.2 Velocity Distribution

As seen in Figure 8a, Figure 9a, and Figure 10a, which visualize the velocity distributions in the downstream, middle, and upstream segments of the dry month discharge, the flow velocity is relatively low throughout the segment, with a maximum velocity of 0.7 m/s. Velocity slows downstream due to the influence of reduced slope and high tide. This also applies to discharge conditions in wet months (Figure 8b, Figure 9b, and Figure 10b) and discharge due to extreme rainfall (Figure 8c, Figure 9c, and Figure 10c). An important observation is that flow velocity increases significantly, especially during discharge due to extreme rainfall. This indicates that extreme rainfall significantly influences discharge, triggering an increase in flow velocity throughout the domain.

In addition to the longitudinal direction, the increase in velocity due to discharge triggered by extreme rainfall also increases in the transverse direction of the river, both on the outer and inner sides. However, the increase in velocity on the outer side is not comparable to the increase on the inner side. This is related to the increase in streamline concentration on the outer side, which is much higher than on the inner side [1]. This results in erosion on the outer side of the bend being more intense than sediment deposition on the inner side of the bend. Secondary currents triggered by changes in flow direction on the outer side of the bend cause much higher flow turbulence in the discharge caused by extreme rainfall, resulting in very high erosive power. Therefore, during high discharge, the intensity of erosion on the outer side of the Palu River bend increases drastically. This confirms the results of a study conducted by Liu et al. [7] dan Santillán et al. [15], where the velocity distribution was non-uniform in both the transverse and longitudinal directions of the river. In general, the density of the streamline tends to be higher on the outside than on the inside of the river channel due to the centrifugal and centripetal forces acting at the river bend and the velocity vector decreases downstream towards the river mouth due to the weakening slope of the energy line [15]. The kinetic energy associated with flow velocity is closely related to the flow's ability to transport sediment. Higher flow velocities have the potential to transport sediment with a large capacity, and often large kinetic energy can cause erosion in the river bed and banks. Conversely, very low flow velocities below the critical velocity of sediment grains have very little transport capacity, causing sediment deposition, especially on the outside of the bend and at the river mouth [16].

A 2D hydrodynamic simulation yields two flow parameters that can be evaluated. The first parameter is the velocity distribution and the other is the flow depth distribution. The flow characteristics can be very well represented by these two parameters [11]. Referring to the simulation results, the velocity distribution can be seen both in the longitudinal direction of the river and in the transverse direction of the river, as shown in Figure 8, Figure 9, and Figure 10.

An interesting observation about the flow characteristics in the study area is the influence of tides in reducing flow velocity at the Palu River estuary. Tidal fluctuations are relatively high, with high water levels (HWL) reaching 2 m based on tidal measurement and generation data. During high tides, flow velocity tends to slow due to a reduced slope of the energy line, which regulates flow movement [23]. Under these conditions, the slope of the energy line can reach zero, creating a flow stagnation point. However, under extreme rainfall conditions, the velocity reduction downstream is not significant due to the small difference between the water level caused by discharge and the high tide, except in normal and low tide conditions.

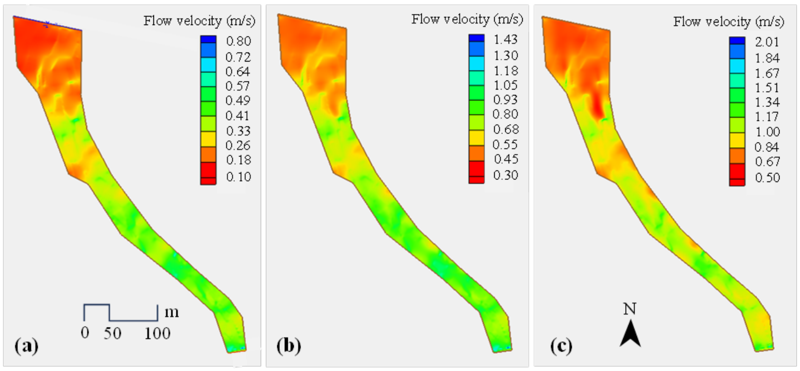

Figure 8. Flow velocity due to discharge in the downstream section of the study area during: (a) dry month; (b) wet month; (c) extreme rainfall

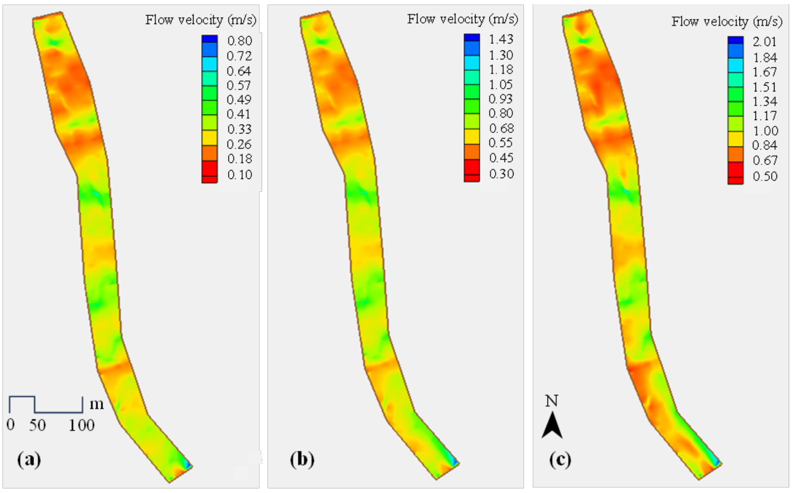

Figure 9. Flow velocity due to discharge in the middle section of the study area during: (a) dry month; (b) wet month; (c) extreme rainfall

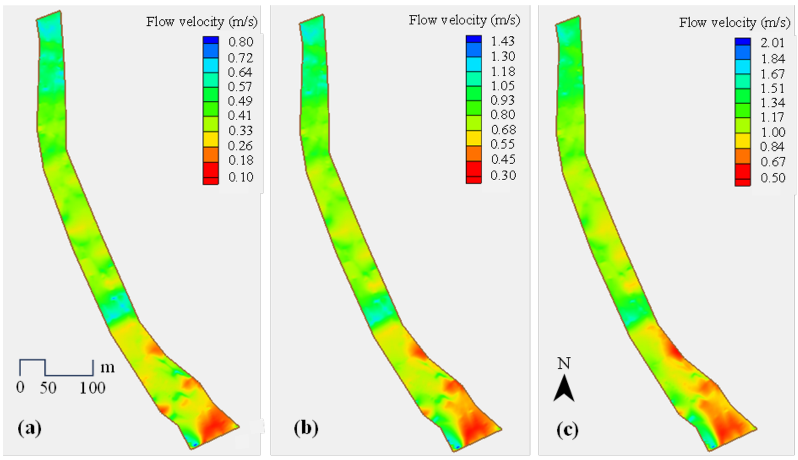

Figure 10. Flow velocity due to discharge in the upstream section of the study area during: (a) dry month; (b) wet month; (c) extreme rainfall

3.3 Water Depth

Changes in water depth are relatively consistent with changes in velocity, where the increase in discharge is proportional to the increase in flow depth in the downstream segment (Figure 11, Figure 12, and Figure 13). The increase increases drastically in discharge in wet months (Figure 11b, Figure 12b, and Figure 13b) and discharge due to extreme rainfall (Figure 11c, Figure 12c, and Figure 13c) compared to flow depth due to discharge in dry months (Figure 11a, Figure 12a, and Figure 13a). In extreme rainfall conditions, the water level can even exceed the elevation of the flood embankments built on the left and right sides of the Palu River.

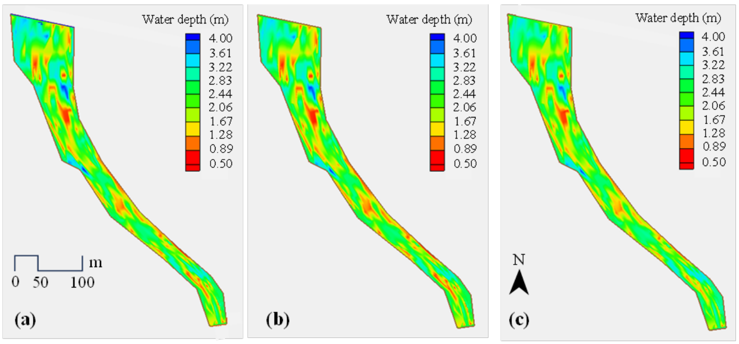

Figure 11. Water depth due to discharge in the downstream section of the study area during: (a) dry month; (b) wet month; (c) extreme rainfall

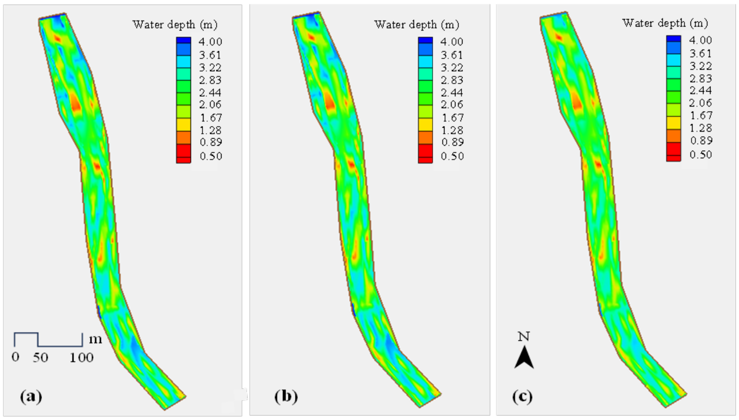

Figure 12. Water depth due to discharge in the middle section of the study area during: (a) dry month; (b) wet month; (c) extreme rainfall

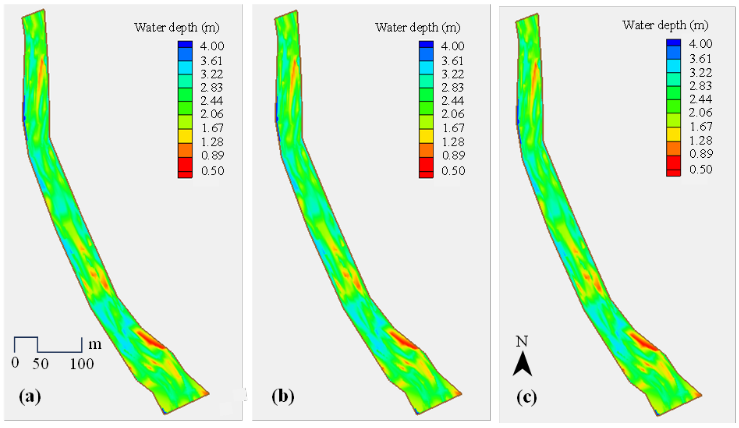

Figure 13. Water depth due to discharge in the upstream section of the study area during: (a) dry month; (b) wet month; (c) extreme rainfall

3.4 Bed Morphology

The main emphasis of this research is to focus on changes in river bed morphology due to extreme rainfall. Increased discharge due to extreme rainfall can be interpreted as an increase in sediment transport, both bed sediment and suspended sediment. Bed sediment with fine and very fine grain sizes is generally transported mostly to the downstream segment of the river. This is related to the large flow carrying capacity along with the increased discharge, so that all fine material, in this case sand, is transported and deposited at the river mouth. The influence of high tides at the river mouth can reduce flow velocity and increase the potential for sediment deposition. This event will occur continuously and fluctuate over time due to the interaction between flow velocity, transported sediment, and downstream boundary conditions controlled by tides. Often, large sedimentation can cause the closure of river outlets and even cause deltas for long periods [23, 30].

Changes in bed elevation in the study area can be observed in both longitudinal and transverse river directions. River bed shallowing is generally found in the downstream segment (Figure 14). The thickness of the deposited sediment layer can reach a maximum of 75 cm, especially at Point P0, and then decreases upstream to Point P600 with a sediment thickness of between 10 cm and 50 cm. Sedimentation at this point is distributed across the entire width of the river, as shown in Figure 15a. Bed shallowing is also confirmed in the middle segment of the river, as illustrated in Figure 15b, with a maximum thickness of 40 cm. This reduction in sediment layer thickness is related to the increasing slope of the river bed, resulting in reduced sedimentation as reported by Tunas et al. [19] and van Emmerik et al. [16]. In addition to bed shallowing, bed degradation occurs in this segment, especially in the upstream section of the studied section. Bed erosion, as shown in Figure 15c, shows a degraded river bed reaching a thickness of 40 cm.

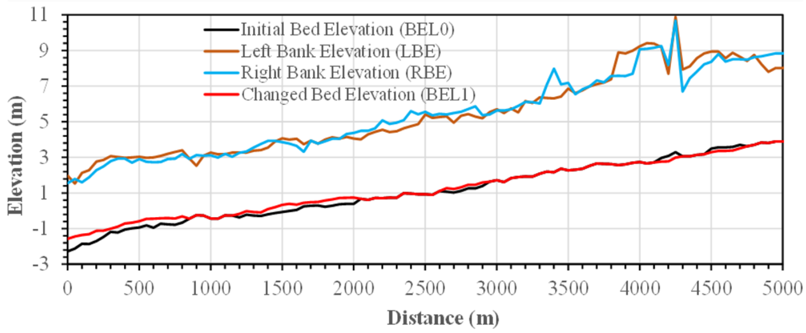

Figure 14. Changes in river bed elevation along the longitudinal direction

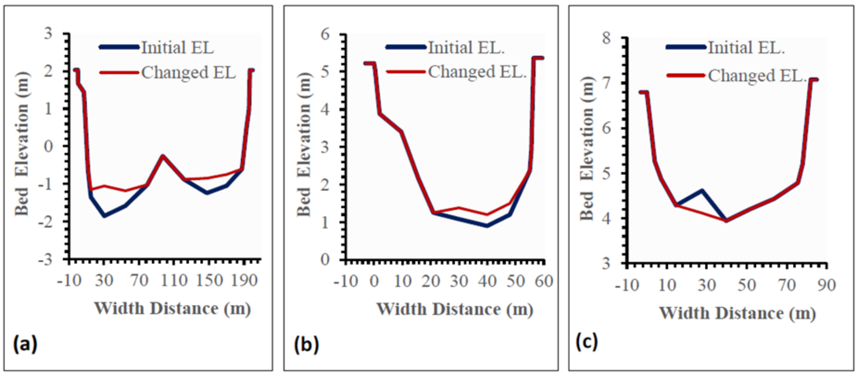

Figure 15. Changes in river bed elevation at cross section direction: (a) CS1 (downstream); (b) CS2 (middle); (c) CS3 (upstream)

4 Conclusions

Aggradation and degradation are the main indicators of changes in alluvial river bed morphology due to the interaction of flow, sediment, and river geometry. River bed morphology changes continuously over time as a hydrodynamic phenomenon in response to flow and sediment fluctuations. These bed morphological changes have been simulated in the downstream segment of the Palu River, one of the major rivers in Central Sulawesi, Indonesia, using the HEC-RAS2D Hydrodynamic Model under discharge input triggered by extreme rainfall. Based on visual observations at the study site, the river bed around the river mouth has become shallower due to massive sedimentation. Sediment material transported with the flow, reduction in river bed slope, and flow stagnation due to high tide levels are considered to be the factors causing these bed morphological changes.

The study results confirmed that the river bed elevation along a 5-km stretch has changed following the flow pattern, geometry, and slope of the river bed. The river bed elevation in the upstream segment was eroded to a maximum depth of 0.40 m, especially on the outer side of the bend, while the segment around the river mouth was sedimented to a maximum height of 0.75 m. The pattern of bed elevation changes due to extreme discharge tends to be similar to the bed elevation changes due to discharge in dry, humid, and wet months, but differs in depth. The bed elevation changes due to extreme discharge are significantly greater than the changes due to discharge in the other three scenarios.

This research can be further developed in relation to its limitations related to the application of 2D models to predict flow velocity and bed morphology changes, where in fact all natural phenomena work in three dimensions. Flow velocity and bed morphology are distributed and changed in 3D directions: longitudinal (x), transverse (y) and vertical (z), where in this study only accommodates the x and y directions. In addition, the neglect of several important parameters such as Coriolis and 3D turbulence effects is an important limitation in this study that can affect streamlines and velocity vectors. Therefore, the assumptions and neglect of these parameters can be accommodated in further research.

Data Availability

The data used to support the findings of this study are available from the corresponding author upon request.

Acknowledgment

This work was officially supported by the Ministry of Higher Education, Science, and Technology through Fundamental Research Grant No. SP DIPA-139.04.1.693320/2025 revisi ke 04. We acknowledge the Directorate of Research and Community Service for providing funding for this research.

Conflicts of Interest

The authors declare that they have no conflicts of interest.

References

[1] Z. Xu, S. Zhang, and X. Yang, “Water and sediment yield response to extreme rainfall events in a complex large river basin: A case study of the Yellow River Basin, China,” *J. Hydrol.*, vol. 597, p. 126183, 2021. https://doi.org/10.1016/j.jhydrol.2021.126183

[2] H. Hamidifar, M. Nones, and P. M. Rowinski, “Flood modeling and fluvial dynamics: A scoping review on the role of sediment transport,” *Earth-Sci. Rev.*, vol. 253, p. 104775, 2024. https://doi.org/10.1016/j.earscirev.2024.104775

[3] A. Paul and M. Biswas, “Changes in river bed terrain and its impact on flood propagation—A case study of river Jayanti, West Bengal, India,” *Geomatics Nat. Hazards Risk*, vol. 10, no. 1, pp. 1928–1947, 2019. https://doi.org/10.1080/19475705.2019.1650124

[4] M. T. Contreras and C. Escauriaza, “Modeling the effects of sediment concentration on the propagation of flash floods in an Andean watershed,” *Nat. Hazards Earth Syst. Sci.*, vol. 20, no. 1, pp. 221–241, 2020. https://doi.org/10.5194/nhess-20-221-2020

[5] S. Thapa, H. D. Sinclair, M. J. Creed, A. G. Borthwick, C. S. Watson, and M. Muthusamy, “Sediment transport and flood risk: Impact of newly constructed embankments on river morphology and flood dynamics in Kathmandu, Nepal,” *Water Resour. Res.*, vol. 60, no. 10, pp. 1–16, 2024. https://doi.org/10.1029/2024WR037742

[6] K. Khosravi, M. Habibnejad, K. Shahedi, A. Chegini, and J. P. Tiefenbacher, “Experimental investigation of bed evolution resulting from dam break,” *J. Hydraul. Struct.*, vol. 6, no. 2, pp. 23–33, 2020. https://doi.org/10.22055/jhs.2020.32713.1131

[7] X. J. Liu, A. J. Kettner, J. Cheng, and S. B. Dai, “Sediment characteristics of the Yangtze River during major flooding,” *J. Hydrol.*, vol. 590, p. 125417, 2020. https://doi.org/10.1016/j.jhydrol.2020.125417

[8] Z. Ziana, A. Azmeri, A. Yulianur, and E. Meilianda, “The eco-hydraulics base as flood mitigation to overcome erosion and sedimentation problems: A case study in the Lae Kombih River, Indonesia,” *J. Water Land Dev.*, vol. 55, pp. 229–239, 2022. http://doi.org/10.24425/jwld.2022.142326

[9] J. Hirschberg, S. Fatichi, G. L. Bennett, B. W. McArdell, N. Peleg, S. N. Lane, and P. Molnar, “Climate change impacts on sediment yield and debris flow activity in an Alpine catchment,” *J. Geophys. Res. Earth Surf.*, vol. 126, no. 1, 2021. https://doi.org/10.1029/2020JF005739

[10] D. H. Lee, E. Cheon, H. H. Lim, S. K. Choi, Y. T. Kim, and S. R. Lee, “An artificial neural network model to predict debris-flow volumes caused by extreme rainfall in the central region of South Korea,” *Eng. Geol.*, vol. 281, p. 105979, 2021. https://doi.org/10.1016/j.enggeo.2020.105979

[11] M. Van Appledorn, M. E. Baker, and A. J. Miller, "River valley morphology, basin size, and flow event magnitude interact to produce wide variation in flooding dynamics," *Ecosphere*, vol. 10, no. 1, p. e02546, 2019. https://doi.org/10.1002/ecs2.2546

[12] M. Reisenbüchler, M. D. Bui, D. Skublics, and P. Rutschmann, "An integrated approach for investigating the correlation between floods and river morphology: A case study of the Saalach river. Germany," *Sci. Total Environ.*, vol. 647, pp. 814–826, 2019. https://doi.org/10.1016/j.scitotenv.2018.08.018

[13] D. Himayoun and T. Roshni, "Geomorphic changes in the jhelum river due to an extreme flood event: A case study," *Arab. J. Geosci.*, vol. 13, p. 23, 2020. https://doi.org/10.1007/s12517-019-4896-9

[14] S. Stähly, M. J. Franca, C. T. Robinson, and A. J. Schleiss, "Erosion, transport and deposition of a sediment replenishment under flood conditions," *Earth Surf. Process. Landf.*, vol. 45, no. 13, pp. 3354–3367, 2020. https://doi.org/10.1002/esp.4970

[15] D. Santillán, L. Cueto-Felgueroso, A. Sordo-Ward, and L. Garrote, "Influence of erodible beds on shallow water hydrodynamics during flood events," *Water*, vol. 12, no. 12, p. 3340, 2020. https://doi.org/10.3390/w12123340

[16] T. H. van Emmerik, R. M. Frings, L. J. Schreyers, R. Hauk, S. I. de Lange, and Y. A. Mellink, "River plastic transport and deposition amplified by extreme flood," *Nat. Water*, vol. 1, pp. 514–522, 2023. https://doi.org/10.1038/s44221-023-00092-7

[17] Y. Du, Z. Cheng, and Z. You, "Morphological changes in a macro-tidal estuary during extreme flooding events," *Front. Mar. Sci.*, vol. 9, p. 1112494, 2023. https://doi.org/10.3389/fmars.2022.1112494

[18] I. G. Tunas, N. Anwar, and U. Lasminto, "A synthetic unit hydrograph model based on fractal characteristics of watersheds," *Int. J. River Basin Manag.*, vol. 17, no. 4, pp. 465–477, 2019. https://doi.org/10.1080/15715124.2018.1505732

[19] I. G. Tunas, P. Harsanto, and Y. Arafat, "Flood mitigation scenario using structural equation modelling (SEM) based on public participation and local wisdom," *Math. Model. Eng. Probl.*, vol. 11, no. 12, pp. 3209–3220, 2024. https://doi.org/10.18280/mmep.111201

[20] I. G. Tunas, "The application of ITS-2 model for flood hydrograph simulation in large-size rainforest watershed, indonesia," *J. Ecol. Eng.*, vol. 20, no. 7, pp. 112–125, 2019. http://dx.doi.org/10.12911/22998993/109882

[21] N. Wang, Q. Chen, K. Hu, K. Xu, S. J. Bentley, and J. Wang, "Morphodynamic modeling of Fourleague Bay in Mississippi River Delta: Sediment fluxes across river-estuary-wetland boundaries," *Coast. Eng.*, vol. 186, p. 104399, 2023. https://doi.org/10.1016/j.coastaleng.2023.104399

[22] I. Aouiche, M. Sedrati, and E. J. Anthony, "Modelling of sediment transport and deposition in generating river-mouth closure: Oum-Errabia River, Morocco," *J. Mar. Sci. Eng.*, vol. 11, no. 11, 2023. https://doi.org/10.3390/jmse11112051

[23] W. Nardin, I. Vona, and S. Fagherazzi, "Sediment deposition affects mangrove forests in the Mekong delta, Vietnam," *Cont. Shelf Res.*, vol. 213, p. 104319, 2021. https://doi.org/10.1016/j.csr.2020.104319

[24] G. Wu, K. Wang, B. Liang, X. Wu, H. Wang, H. Li, and B. Shi, "Modeling the morphological responses of the Yellow River Delta to the water-sediment regulation scheme: The role of impulsive river floods and density-driven flows," *Water Resour. Res.*, vol. 59, no. 7, 2023. https://doi.org/10.1029/2022WR033003

[25] T. M. Basuki, H. Y. S. H. Nugroho, Y. Indrajaya, I. B. Pramono, N. P. Nugroho, A. B. Supangat, and D. P. Simarmata, "Improvement of integrated watershed management in Indonesia for mitigation and adaptation to climate change: A review," *Sustainability*, vol. 14, no. 16, p. 9997, 2022. https://doi.org/10.3390/su14169997

[26] X. Li, Q. Hu, Q. Zhang, and R. Wang, "Response of rainfall erosivity to changes in extreme precipitation in the Poyang Lake Basin, China," *J. Soil Water Conserv.*, vol. 75, no. 4, pp. 537–548, 2020. https://doi.org/10.2489/jswc.2020.00203

[27] Y. Yao, J. Liu, Z. Wang, X. Wei, H. Zhu, W. Fu, and M. Shao, "Responses of soil aggregate stability, erodibility and nutrient enrichment to simulated extreme heavy rainfall," *Sci. Total Environ.*, vol. 709, p. 136150, 2020. https://doi.org/10.1016/j.scitotenv.2019.136150

[28] S. Dang, X. Liu, H. Yin, and X. Guo, "Prediction of sediment yield in the middle reaches of the Yellow River Basin under extreme precipitation," *Front. Earth Sci.*, vol. 8, p. 542686, 2020. https://doi.org/10.3389/feart.2020.542686

[29] M. F. Yass and A. Al-Tikrite, "Sediment characteristics of the riverbed: The Tigris River case (Iraq)," *Math. Model. Eng. Probl.*, vol. 12, no. 6, pp. 2077–2084, 2025. https://doi.org/10.18280/mmep.120623

[30] B. Das and T. S. Vadivel, "Sediment transport modelling in stream flow by HEC-RAS model—A state-of-the-art," in *Lecture Notes in Civil Engineering*, 2022, pp. 481–491. https://doi.org/10.1007/978-981-19-0189-8_39

[31] A. M. Juma'a, "Numerical solution for both steady and unsteady state of fluid flow between two heated parallel walls," *Int. J. Comput. Methods Exp. Meas.*, vol. 12, no. 1, pp. 77–82, 2024. https://doi.org/10.18280/ijcmem.120109

Nomenclature

h	mater level, m
q	suspended sediment transport, kg·m^{-1}·s^{-1}
C	sediment concentration, kg·m-3
D	deposition rate, kg·m^{-2}·s
E	erosion rate, kg·m^{-2}·s
U	current velocity, m·s^{-1}
HF	hydraulic flow erosion
SS	sheet and splash erosion
DEM	digital elevation model
HEC	hydrologic engineering center
HMS	hydrologic modeling system
HWL	high water levels, m
RAS	river analysis system
LULC	land use land cover
RMSE	root mean square error
Greek symbols	
∂	partial derivative operator
β	correction factors
ε	diffusion coefficient, m^2·s^{-1}
φ	porosity of deposited and degraded materials
κ	empirical parameter
ρ	particle density, kg·m^{-3}
τ	critical shear stress, kg·m·sec^2
∇	vector differential operator
Subscripts	
b	bed
k	size class, mm
t	time, s
bn	bed-load secondary flow
bk	bed-load sediment
sk	suspended-load sediment
tk	total-load sediment
zb	bed elevation, m
bhk	horizontal diffusion coefficient of bed-load, m^2·s^{-1}